OPEN ACCESS INTERNATIONAL JOURNAL OF SCIENCE & ENGINEERING

SYNTHESIS AND CHARATERIZATION OF MONOETHANOLAMINE CAPPED CERIUM OXIDE NANOPARTICLES

Biju Joy
Department of Chemistry, St. Xavier's College, Thumba, Trivandrum, India.
bijujoysjc@gmail.com

Abstract: **The Monoethanolamine (MEA) capped Cerium oxide Nanoparticles (CeO_2 NPs) was synthesized by co-precipitation method. Synthesized MEA capped CeO_2 NPs was formed face centered cubic structure. The morphological and elemental analyses were carried out using FESEM and EDAX spectrum. Various functional characteristic peaks were observed FT-IR spectrum. From the UV-Vis spectrum, the absorption edge peak was found to be 317 nm for MEA capped CeO_2 NPs. The photoluminescence measurements revealed that the broad emissions were composed of five different peaks observed for MEA capped CeO_2 NPs.**

Keywords: *CeO_2 NPs; Monoethanolamine; XRD; FESEM.*

---∴∴∴---

I INTRODUCTION

Cerium oxide (CeO_2) are important nanoparticles for a various types of applications in catalysts [1, 2], fuel cell [3], chemical-mechanical polishing for microelectronics, phosphor/ luminescence [4], and metallurgical and glass/ceramic applications. In literature CeO_2 NPs have been synthesized by various methods, sol-gel processing [5,6], hydrothermal synthesis [7–10], homogeneous precipitation with urea or hexamethylenetetramine [11,12], flame spray pyrolysis [13], a reverse micelles route [14,15], combustion synthesis [16], sonochemical and microwave-assisted heating routes [17], egg white solution route [18], a complex thermo-decomposition method [19], and co-precipitation method [20]. Among the various methods, co-precipitation is one of the most important methods to prepare the nanoparticles. The co-precipitation method reduces the temperature of the reaction where a homogeneous mixture of reagent precipitates. It is a simple method for the synthesis of nanopowders of metal oxides, which are highly reactive in low temperature sintering.

In the present studies, Monoethanolamine (MEA: $[CH_2 (OH) CH_2] NH$) is selected for capping with CeO_2 NPs. The reason is that the amino group of MEA having more energy to give the charge transfer (CT) for electronic absorption corresponding to the transition from the ground to the first excited state. MEAcapping CeO_2 NPs is prepared through the co-precipitation method. The synthesized MEAcapping CeO_2 NPs is characterized by X-ray diffraction (XRD), Field Emission Scanning Electron Microscopy (FESEM),Energy dispersive analysis X-ray (EDAX). The functional groups are identified using Fourier Transform Infra-Red (FT-IR). The optical studies were carried out by UV-VIS and Photoluminescence spectrum.

II MATERIALS AND METHOD

The following high purity chemicals such as cerium nitrate, Monoethanolamine (MEA), and Sodium hydroxide were used as precursors without further purification.

The MEA added CeO_2 NPs synthesis following, Cerium Nitrate0.1 M with a capping agent added MEA 0.05M were dissolved double distilled water separate 100ml beaker, then form a homogenous mixture. 0.8 M of NaOH was separately dissolved in 100 ml of double distilled water. Then, NaOH solution was added drop wise to the homogenous mixture of Cerium nitrate solution, the pH 12.30 obtained and which yields violet precipitate. The solution with the violet precipitate was stirred at room temperature for 6 h. This solution was refluxed at room temperature for 24 h. Then, a clear solution was obtained, which found to be stable at ambient condition. Thereafter, the solution was washed several times with double distilled water and ethanol. The precipitate was dried at 120 $^{\circ}$C. Finally, MEA capped CeO_2 samples were annealed at the 700 ^{o}C for 5 h because the energy from the heat could enhance the vibration and diffusion of lattice atoms for atomic re-arrangements.

A. Characterization Techniques

The MEA capped CeO_2 NPs was characterized by X-ray diffractometer (model: X'PERT PRO PANalytical). The diffraction patterns were recorded in the range of 30°-80° for the MEA capped CeO_2 NP samples where the monochromatic wavelength of 1.54 Å was used. The samples were analyzed by Field Emission Scanning Electron Microscopy (Carl Zeiss Ultra 55 FESEM) with EDAX (model: Inca). The FT-IR spectra were recorded in the range of 400-4000 cm^{-1} by using a Perkin-Elmer spectrometer. The absorption spectra of MEA capped CeO_2 NPs samples were studied in the range between 200 and 1100 nm of Lambda 35 spectrometer. Photoluminescence spectra were studied using a Perkin Elmer-LS 14.

III RESULTS AND DISCUSSION

B. X-ray diffraction pattern studies

Figure 1 shows that X-ray diffraction pattern of MEA capped CeO_2 NPs. The synthesized MEA capped CeO_2 NPs are exhibits face, center cubic structure with the lattice parameters a = b = c = 5.411 Å and α = β = γ = 90°. The indexed XRD peaks are found to be (111), (200), (220), (311), (222), (400) and (331) corresponding (2θ) angle at 28.586˚, 33.132 ˚, 47.534 ˚, 56.383 ˚, 59.09 ˚, 69.46 ˚ and 76.73 ˚ well matched with the standard diffraction data JCPDS No: 34-0394.

The lattice parameters CeO_2 NPs is calculated according to the formula

$$\frac{1}{d^2} = \left(\frac{h^2 + k^2 + l^2}{a^2}\right)$$

The lattice constant 'a' value is obtained through the relation $a = \sqrt{d^2(h^2 + k^2 + l^2)}$. The calculated 'a' value is 5.4041 Å, for MEA capped CeO_2 NPs respectively.

The average crystallite size of the MEA capped CeO_2 NPs are calculated by Debye Scherrer's relation

Average crystallite size $D = \frac{k\lambda}{\beta_{D}\cos\theta}$

Where, λ is the wavelength of the radiation (1.54056 Å for CuKα radiation), k is a constant which is equal to 0.94, β is the peak width at half-maximum intensity, θ is the peak position. The average crystallite sizes are found to be 21.56 nm for MEA capped CeO_2 NPs respectively.

Figure 2 (a-b) shows the FESEM image high and low magnification images of MEA capped CeO_2 NPs. The morphology of the synthesized CeO_2 NPs is formed spherical structure and particles are present in the nanometer scale. Elemental compositions are identified using EDAX spectra for synthesized MEA capped CeO_2 NPs as shown in Fig. 2(c). In the present work, the chemical compositions of Ce and O atomic percentage are observed at 31.13 % and 68.87% for MEA capped CeO_2 NPs.

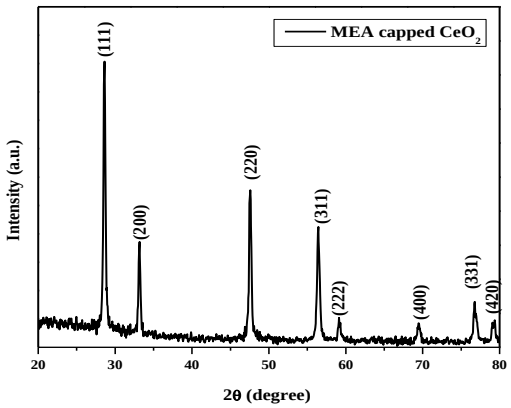

Figure 1: X-ray diffraction pattern of MEA capped CeO_2 NPs

C. Morphological and Elemental composition of MEA capped CeO_2 NPs

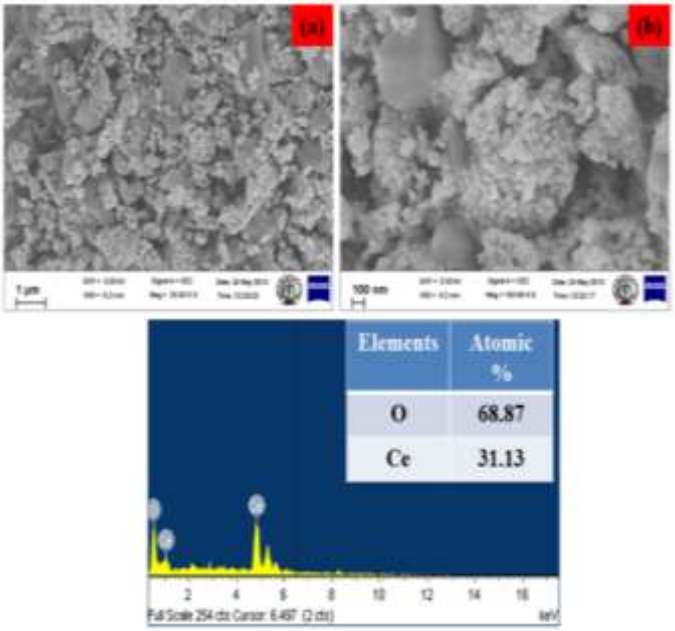

Figure 2: (a-c) Morphological and elemental analysis of MEA capped CeO_2 NPs

D. FT-IR spectroscopic studies

FT-IR spectrum of MEA capped CeO_2 NPs is shown in Fig. 3. The broad absorption O-H peak observed at 3750-3000 cm^{-1} [21]. From the FTIR result, the O-H stretching of residual alcohols, water and Ce-OH found to 3422 cm^{-1} for MEA capped CeO_2 NPs. The C-H characteristic band is found to be 2939 cm^{-1} [22]. The absorption band at 1641 cm^{-1} is ascribed O-H symmetric stretching for MEA capped CeO_2 NPs [22]. The Ce-O-Ce is stretching, vibration observed at 1008 cm^{-1}. The Ce-O-C bending mode vibration is observed at 687 cm^{-1} for MEA capped CeO_2 NPs [23,24]. The strong Ce-O stretching vibration is found to be 505 cm^{-1} for MEA capped CeO_2 NPs.

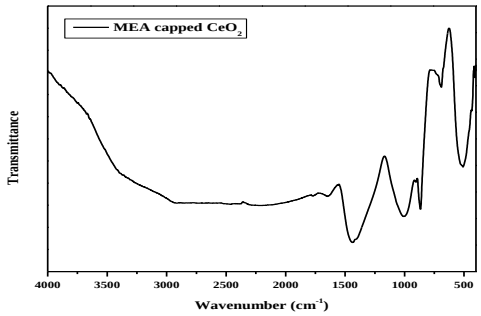

Figure 3: FT-IR spectrum of MEA capped CeO_2 NPs

E. UV-Vis spectroscopic studies

The UV-Vis absorption spectrum of MEA capped CeO_2 NPs is shown in Fig. 4. The absorption edge peak is observed at 317 nm for MEA capped CeO_2 NPs. This is due to the photo excitation of electron from the valence band to conduction band.

The relation between the absorption coefficients α and the incident photon energy hυ can be written as

$\alpha h\upsilon = A(h\upsilon - E_g)^n$

Where E_g is the optical band-gap. A is a constant and the exponent n depends on the transition. The value of (n = 1/2, 3/2, 2, or 3) depends on the nature of the electronic transition (1/2 for allowed direct transition, 2 for allowed in-direct transition, 3/2 and 3 for forbidden direct and forbidden indirect transitions, respectively). Considering direct and indirect band transition in NPs, a plot between $(\alpha h\upsilon)^{2 \text{ and } 1/2}$ Vs. hυ and extrapolating the linear portion of the absorption edge to find the intercept with energy axis is shown in Fig. 5. Estimated band gap of MEA capped CeO_2 NPs values observed at 2.95 eV and 2.45 eV respectively. The CeO_2 NP sample shows a decrease in E_g by a value exceeding 0.24, as compared to the bulk CeO_2powders (Eg = 3.19 eV (direct), determined by UV-Visible spectroscopy) [25]. For the reason of decrease in the optical band gap of CeO_2. The band gap MEA capped CeO_2 red shift occurred as compared to that of the bulk CeO_2.The red-shift in the band gap can be attributed to the Ce^{3+} at the grain boundaries. This may be arrangements of some localized gap states in the band gap [26, 27].

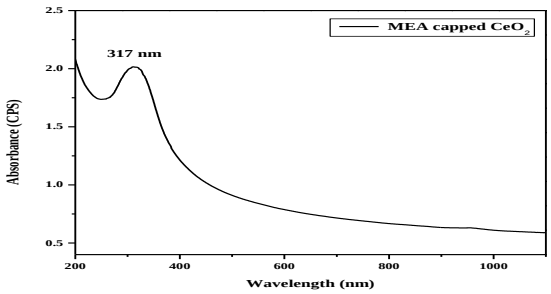

Figure 4: UV-Visible spectra of the MEA capped CeO_2 NPs

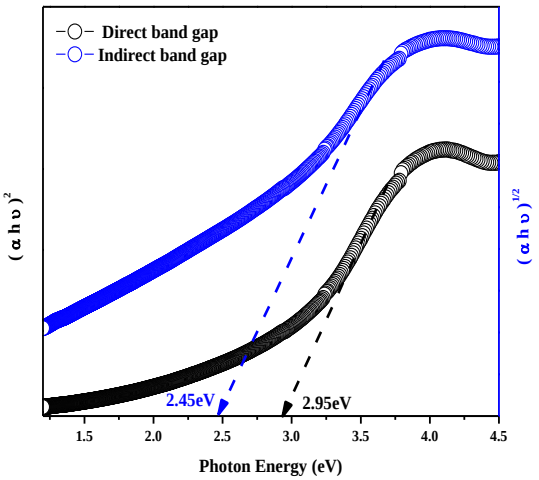

Figure 5: Direct and indirect band gaps of MEA capped CeO_2 NPs

F. Photoluminescence spectroscopic studies

Figure 6 shows the room temperature photoluminescence emission spectrum of MEA capped CeO_2 NPs. The as-synthesized CeO_2 NPs was observed in the excited wavelength 325 nm. Murugan et al., (2017) reported that the PL emission values are (361 nm, 378 nm, 391 nm, 408 nm, 450 nm, 490 nm and 520 nm) for CeO_2 NPs [28]. The emission spectrum of the MEA capped CeO_2 NPs peaks are observed at 366 nm, 390 nm, 415 nm, 459 nm and 485 nm respectively. The two UV emission peaks observed at 366 nm and 390 nm are corresponding to the near band edge (NBE) emission, this is due to the recombination of free excitons [28]. The violet emission center at 415 nm, it's attributed to the charge transitions from the 4f band to the valance band of CeO_2 [29]. Blue emission observed at 459 nm, which is due to the localization of the energy levels among the Ce 4f and O 2p bands. The blue-green emission located at 485 nm, is ascribed to surface defects. From the PL emission values (366 nm, 390 nm, 415 nm, 459 nm and 485 nm) are decreased as compared to the early literature (361 nm, 378 nm, 391 nm, 408 nm, 450 nm, 490 nm and 520 nm) emission values of CeO_2 NPs [28]. These blue shift may occur from different origins, such as electron phonon coupling, lattice distortion, localization of charge carriers due to interface effects and point defects. In PL spectrum the defect level emission was reduced MEA capped CeO_2 NPs. The optoelectronic properties mainly depend on the reduction of the defect level in material, which influenced by electron phonon coupling interaction. In the present investigation, MEA capped CeO_2 NPs defect level was decreased. In PL results provides strong support for the further development of extensive optical device applications.

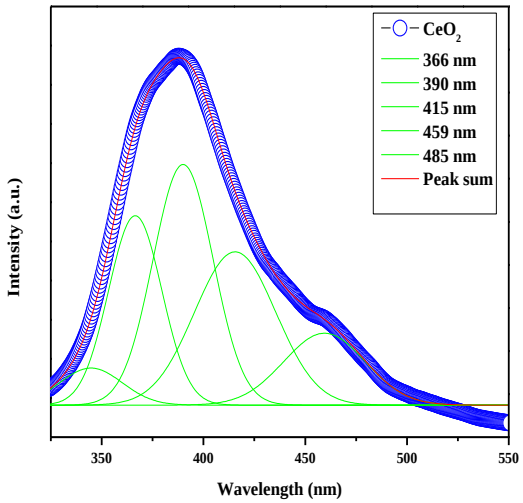

Figure 6: Photoluminescence spectra of MEA capped CeO_2 NPs

IV CONCLUSIONS

In summary, MEA capped CeO_2 NPs prepared through co-precipitation method. The XRD patterns confirmed that the synthesized MEA capped CeO_2 NPs was exhibited cubic phase. From the FESEM image, the synthesized CeO_2 NPs was formed spherical structure. Elemental compositions were identified using EDAX spectrum. In FT-IR spectrum, Ce-O stretching vibration was observed at 505 cm^{-1} for MEA capped CeO_2 NPs. The UV-Vis spectrum, the estimated direct and indirect band gaps of MEA capped CeO_2 NPs values found to be 2.95 eV and 2.45 eV respectively. From the PL spectrum, the defect level emission was reduced MEA capped CeO_2 NPs. The optoelectronic properties mainly depended on reduction the of defect level in material, which influenced by electron phonon coupling interaction. In the present work, MEA capped CeO_2 NPs defect level was decreased. In PL results provides strong support for the further development of extensive optical device applications.

REFERENCES

[1] Mogensen M, Sammes NM, Tompsett GA. Physical, chemical and electrochemical properties of pure and doped ceria. Solid State Ionics. 2000 Apr 30;129(1):63-94.

[2] Yashima M, Sasaki S, Yamaguchi Y, Kakihana M, Yoshimura M, Mori T. Internal distortion in ZrO_2–CeO_2 solid solutions: neutron and high-resolution synchrotron x-ray diffraction study. Applied physics letters. 1998 Jan 12;72(2):182-4.

[3] Nikolaou K. Emissions reduction of high and low polluting new technology vehicles equipped with a CeO_2 catalytic system. Science of the total environment. 1999 Sep 1;235(1):71-6.

[4] Ozawa M. Role of cerium–zirconium mixed oxides as catalysts for car pollution: A short review. Journal of alloys and compounds. 1998 Jul 24;275:886-90.

[5] Alifanti, M., Baps, B., Blangenois, N., Naud, J., Grange, P. and Delmon, B., 2003. Characterization of CeO_2−ZrO_2mixed oxides. Comparison of the citrate and sol−gel preparation methods. *Chemistry of Materials*, *15*(2), pp.395-403.

[6] Laberty-Robert, C., Long, J.W., Lucas, E.M., Pettigrew, K.A., Stroud, R.M., Doescher, M.S. and Rolison, D.R., 2006. Sol−Gel-Derived Ceria Nanoarchitectures: Synthesis, Characterization, and Electrical Properties. *Chemistry of materials*, *18*(1), pp.50-58.

[7] Hirano M, Inagaki M. Preparation of monodispersed cerium (IV) oxide particles by thermal hydrolysis: influence of the presence of urea and Gd doping on their morphology and growth. Journal of Materials Chemistry. 2000 Jan 1;10(2):473-7.

[8] Hirano M, Kato E. Hydrothermal synthesis of cerium (IV) oxide. Journal of the American Ceramic Society. 1996 Mar 1;79(3):777-80.

[9] Hirano M, Fukuda Y, Iwata H, Hotta Y, Inagaki M. Preparation and spherical agglomeration of crystalline cerium (IV) oxide nanoparticles by thermal hydrolysis. Journal of the American Ceramic Society. 2000 May 1;83(5):1287-9.

[10] Zhou Y, Rahaman MN. Effect of redox reaction on the sintering behavior of cerium oxide. Acta materialia. 1997 Sep 1;45(9):3635-9.

[11] Chu X, Chung WI, Schmidt LD. Sintering of Sol-Gel- Prepared Submicrometer Particles Studied by Transmission Electron Microscopy. Journal of the American Ceramic Society. 1993 Aug 1;76(8):2115-8. [12] Chen PL, Chen IW. Reactive cerium (IV) oxide powders by the homogeneous precipitation method. Journal of the American Ceramic Society. 1993 Jun 1;76(6):1577-83.

[13] Mädler L, Stark WJ, Pratsinis SE. Flame-made ceria nanoparticles. Journal of Materials Research. 2002 Jun;17(6):1356-62.1356.

[14] Masui, T., Fujiwara, K., Machida, K.I., Adachi, G.Y., Sakata, T. and Mori, H., 1997. Characterization of cerium (IV) oxide ultrafine particles prepared using reversed micelles. *Chemistry of Materials*, *9*(10), pp.2197-2204.

[15] Sathyamurthy S, Leonard KJ, Dabestani RT, Paranthaman MP. Reverse micellar synthesis of cerium oxide nanoparticles. Nanotechnology. 2005 Jul 28;16(9):1960.

[16] Mokkelbost T, Kaus I, Grande T, Einarsrud MA. Combustion synthesis and characterization of nanocrystalline CeO2-based powders. Chemistry of materials. 2004 Dec 14;16(25):5489-94.

[17Maensiri S, Masingboon C, Laokul P, Jareonboon W, Promarak V, Anderson PL, Seraphin S. Egg white synthesis and photoluminescence of platelike clusters of CeO2

nanoparticles. Crystal growth & design. 2007 May 2;7(5):950-5.
[18] Li L, Chen Y. Preparation of nanometer-scale CeO 2 particles via a complex thermo-decomposition method. Materials Science and Engineering: A. 2005 Oct 15;406(1):180-5.
[19] Liao, X.H., Zhu, J.M., Zhu, J.J., Xu, J.Z. and Chen, H.Y., 2001. Preparation of monodispersed nanocrystalline CeO_2 powders by microwave irradiation. *Chemical Communications*, (10), pp.937-938.
[20] Jalilpour M, Fathalilou M. Effect of aging time and calcination temperature on the cerium oxide nanoparticles synthesis via reverse co-precipitation method. International Journal of Physical Sciences. 2012 Feb 2;7(6):944-8.
[21] Choudhury B, Chetri P, Choudhury A. Annealing temperature and oxygen-vacancy-dependent variation of lattice strain, band gap and luminescence properties of CeO_2 nanoparticles. Journal of Experimental Nanoscience. 2015 Jan 22;10(2):103-14.
[22] Murugan, R., Ravi, G., Vijayaprasath, G., Rajendran, S., Thaiyan, M., Nallappan, M., Gopalan, M. and Hayakawa, Y., 2017. Ni–CeO_2 spherical nanostructures for magnetic and electrochemical supercapacitor applications. *Physical Chemistry Chemical Physics*, *19*(6), pp.4396-4404.
[23] Sujana MG, Chattopadyay KK, Anand S. Characterization and optical properties of nano-ceria synthesized by surfactant-mediated precipitation technique in mixed solvent system. Applied Surface Science. 2008 Sep 15;254(22):7405-9.
[24] dos Santos G, Simmonds AJ, Krause HM. A stem-loop structure in the wingless transcript defines a consensus motif for apical RNA transport. Development. 2008 Jan 1;135(1):133-43.
[25] Orel ZC, Orel B. Optical properties of pure CeO2 and mixed CeO2/SnO2 thin film coatings. physica status solidi (b). 1994 Nov 1;186(1).
[26] Choudhury B, Choudhury A. Ce^{3+} and oxygen vacancy mediated tuning of structural and optical properties of CeO_2nanoparticles. Materials Chemistry and Physics. 2012 Jan 5;131(3):666-71.
[27] Patsalas, P., Logothetidis, S., Sygellou, L. and Kennou, S., 2003. Structure-dependent electronic properties of nanocrystalline cerium oxide films. *Physical Review B*, *68*(3), p.035104.
[28] Wang L, Ren J, Liu X, Lu G, Wang Y. Evolution of SnO_2 nanoparticles into 3D nanoflowers through crystal growth in aqueous solution and its optical properties. Materials Chemistry and Physics. 2011 May 16;127(1):114-9.
[29] Murugan, R., Vijayaprasath, G., Mahalingam, T. and Ravi, G., 2016. Enhancement of room temperature ferromagnetic behavior of rf sputtered Ni-CeO_2 thin films. Applied Surface Science, 390, pp.583-590.